Comparison of 4.5 Hz Geophones and a Broadband Seismometer in a Real Field Deployment

Tyler Rasmussen

Thesis submitted to the faculty of the Virginia Polytechnic Institute and State University
in partial fulfillment of the requirements for the degree of

Master of Science
In
Geosciences

John A. Hole

Martin C. Chapman

Ying Zhou

Feb 20, 2019

Blacksburg, Virginia

Keywords: Geophones, Broadband seismometers, Dense Arrays

Comparison of 4.5 Hz Geophones and a Broadband Seismometer in a Real Field Deployment

Tyler Rasmussen

ABSTRACT

An analysis of waveforms, power spectral density and array responses was performed using geophones and broadband seismometers, codeployed as part of a geologically motivated study. Broadband seismometers record excellent waveforms but, due to cost and deployment effort, wavefields are usually spatially aliased above ~0.1 Hz. Industry rapidly deploys many thousands of inexpensive, passive geophones to record full, unaliased seismic wavefields; however, waveform quality is limited below the instrument's natural frequency of ≥2 Hz. In 2012, coincident passive and controlled-source seismic surveys were deployed to investigate tectonics in Idaho and Oregon. Broadband stations were deployed at quiet sites every 15 km, taking experienced professionals >1 person-days per station. Fifty 4.5 Hz geophones and "Texan" seismographs at 200-m spacing were deployed per person-day by inexperienced students. Geophone data were continuously recorded for 3 nights and 1 day, while broadband seismometers were deployed for ~2 years. The spectral and array responses of these real deployments were compared. For a M7.7 teleseismic event, the broadband seismometer and geophone recorded nearly identical waveforms down to <0.03 Hz (32 s) and matching power spectral density down to 0.02 Hz (50 s). For quiet ambient noise, the waveforms strongly correlate down to <0.25 Hz (4 s) and the power spectral density match to the low-frequency side of the microseismic peak at ~0.15 Hz (~7 s). By deploying a much larger number of geophones, waveforms can be stacked to reduce

instrument self-noise and beamforming can be used to identify wavefield azimuth and apparent velocity. Geophones can be an effective tool in ambient noise seismology down to ~7 seconds and can be used to record large seismic events effectively down to tens of seconds, well below the natural frequency of the instruments. A well-designed deployment of broadbands and geophones can enable full wavefield studies from long period to short period. Scientific and societal applications that could benefit from the improved unaliased wavefield bandwidth include local to regional seismicity, strong ground motion, magma migration, nuclear source discrimination, and crustal studies.

GENERAL AUDIENCE ABSTRACT

An analysis of seismic responses was performed using common seismology sensors, codeployed as part of a geologically motivated study. Broadband seismometers record seismic activity extremely well, however, due to cost and deployment effort, are less effective above ~0.1 Hz. Industry rapidly deploys many thousands of inexpensive, geophones, to record effectively above ~2 Hz; however, quality of the signal is limited below 2 Hz. In 2012, coincident seismic surveys were deployed to investigate earth structures in Idaho and Oregon. Broadband stations were deployed at every 15 km, taking experienced professionals >1 person-days per station. Fifty geophones and "Texan" seismographs at 200-m spacing were deployed per person-day by inexperienced students. Geophone data were continuously recorded for 3 nights and 1 day, while broadband seismometers were deployed for ~2 years. The seismic responses of these real deployments were compared. For a M7.7 earthquake, the broadband seismometer and geophone recorded nearly identical waveforms down to <0.03 Hz (32 s) and had similar characteristics down to 0.02 Hz (50 s). For low energy seismic signal, the waveforms were comparable down to <0.25 Hz (4 s) and had similar characteristics at ~0.15 Hz (~7 s). By deploying a much larger number of geophones, waveforms can be added together to improve signal quality and determine where the seismic source is located. Geophones can be an effective tool for low energy seismic signal down to ~7 seconds in period and can be used to record large seismic events effectively down to tens of seconds in period. A well-designed deployment of broadbands and geophones can enable full seismic studies from low and high frequencies which would have many scientific and societal benefits.

ACKNOWLEDGEMENTS

I would like to thank my advisor, Dr. John Hole, for his continued guidance, instruction, and support with my research at Virginia Tech. I would also like to thank Dr. Martin Chapman and Dr. Ying Zhou for acting as my committee members for my master's degree and for their insightful comments and suggestions for my research.

Thanks to Dr. John Hole, Dr. Christian Stanciu, Dr. Kathy Davenport, and Dr. Ray Russo and the rest of the IDOR research group who were involved in the collection of the data used in this thesis. Additional thanks go to Dr. John Hole, Dr. Christian Stanciu, Dr. Kathy Davenport, and Dr. Martin Chapman who were extremely helpful in troubleshooting problems that arose during processing of the seismic data.

IDOR seismic data were acquired with support from National Science Foundation grants, EAR-0844187 to R. M. Russo and EAR-0844264 to J. A. Hole. The seismic instruments were provided by the Incorporated Research Institutions for Seismology (IRIS) through the PASCCAL Instrument Center at New Mexico Tech. The seismic data are archived and available through the IRIS Data Management Center. Seismic Analysis Code (SAC) was used for data processing.

I would also like to offer a special thanks to my family: first and foremost, my wife, Kiera Rasmussen, who joined me and continually supported me during my time at Virginia Tech. I would also like to thank my parents, Eric and Michelle Rasmussen for their support and encouragement during my entire education process, as well as my wife's family, Bret and Karilee Barfuss, for their support.

TABLE OF CONTENTS

Introduction

Larger seismic deployments are being enabled by the recent development, by industry, of standalone, non-cabled, geophones and continuously recording seismograph systems called "nodes" (Karplus and Schmandt, 2018). The power density of batteries is rapidly improving, the power demand of recording systems is decreasing, and memory storage is growing rapidly, driven by commercial electronics. Therefore, smaller, less expensive seismographs are needed for long-duration continuous recording. Unlike long-period, active seismometers, short-period, passive seismometers like geophones require no power. Consequently, these short-period geophones are less expensive, smaller, lighter, can be quickly deployed (e.g. Davenport et al., 2015), and require significantly less power than previous generations of seismometers and seismographs. These advantages allow for larger and denser deployments of stations which reduce spatial aliasing and record more of the full wavefield.

Dense arrays of geophones have long been used by industry to record controlled-source reflection and refraction full seismic wave fields that are not spatially aliased (e.g., Sheriff and Geldart, 1995). Generally, controlled-source applications are used to image between 5 Hz and 1 kHz frequencies. The current petroleum industry standard is to deploy tens of thousands of short-period geophone channels. The inherent disadvantage for the short-period geophone nodes is that the sensitivity of the instruments to ground motion decreases rapidly below the instrument's corner frequency, leading to ineffectiveness at long periods (Rodgers, 1994). Passive seismometers become large and heavy for natural frequencies below 1 Hz, so, actively powered intermediate and long-period seismometers have long been preferred for earthquake seismology below 1 Hz. This includes broadband seismometers that record from 25 Hz to <0.003 Hz (>300 s). The high cost, weight, and power demands of intermediate-period and

broadband seismometers limits the number of stations and density that can be practically deployed. That number is currently around 100 stations which results in arrays that are often badly spatially aliased at shorter periods, > 0.2 Hz (< 5 s). Smaller station spacing can be deployed, but at the cost of diminished spatial coverage which is often needed for long periods and long wavelengths.

There are many applications in seismology which fall between the frequencies that are commonly recorded by geophones and the frequencies where broadband seismometer arrays are not spatially aliased. These applications fall between roughly 0.1 Hz and 10 Hz (0.1-10 s) and have scientifically and societally important impacts including earthquake hazards and building resonant frequencies (e.g., Gallipoli et al., 2010; Hong and Hwang, 2000; Snieder and Safak, 2006), long-period volcano magma migration (e.g. Almendros et al. 2002; Montalto, 1995), and source characterization and discrimination (e.g., Al-Eqabi et al., 2001). These applications and other basin to crustal scale studies would benefit from practical field instrumentation, which could record the unaliased seismic wavefield.

Seismometers can record below their natural frequency, however, they become exponentially less sensitive to small ground shaking and sensor self-noise becomes larger than the seismic signal (Rodgers, 1994). With sufficiently large signal, seismometers can record far below their natural frequency. For example, Chapman (2009), showed that a 1 Hz passive seismometer records signal identical to a broadband seismometer down to a frequency of 0.1 Hz (10 s), which is sufficient sensitivity to record local and regional earthquakes. Data below the natural frequency from geophone nodes has been used successfully in ambient noise (e.g. Lin et al., 2013; Ranasinghe et al., 2018; Wang et al., 2017), receiver functions (e.g., Liu et al., 2018),

volcano studies (e.g., Hansen and Schmandt, 2015; Glasgow et al., 2018; Brenguier et al., 2016), and microseismic event detection (e.g. Trow et al., 2018).

Laboratory shake table (e.g., Rogers, 1994), vault (e.g., Chapman, 2009) and field test site studies have quantified the response of geophones at lower frequencies. These studies are done in controlled, optimal environments. To my knowledge, a quantitative comparison of geophones and broadbands in a realistic, geologically motivated field deployment has not been published. Realistic, geologically motivated field deployments for scientist-led research are rarely deployed at the same quality as vault deployments. This is due to limitations of cost, time and site availability which affect every scientist-led large array research project. The deployment of many stations to reduce aliasing requires streamlining cost and field logistics, resulting in poorer quality of deployments. The field cost of temporary arrays often limits burial to very small concrete pads or direct burial. Denser station spacing, permitting, and limited funds often result in station locations near noise sources, further from bedrock and shallow buried stations in loose soil. To deploy many stations, geophone nodes are deployed rapidly with less care and sites are chosen based on permitting or access instead of quality of site. Large, inexperienced crews are often used with long days and exhaustion affecting work quality. These challenges are not encountered in lab, vault, and single-station field tests, and the compromises in quality do not have to be made.

This study compares geophone nodes to a broadband seismometer deployed during a geologically motivated research project. A large broadband teleseismic array and a large controlled-source geophone node array were co-deployed as part of the Earthscope Idaho-Oregon project (IDOR) to study regional tectonics (Stanciu et al., 2016; Davenport et al., 2017, Tikoff et al., 2017; Bremner et al., 2019). The goal of this study is to determine the minimum

frequency that can be recorded by realistically deployed geophone nodes, comparable to a broadband station. This can inform future co-deployment of geophone nodes and broadband stations to improve spatial sampling.

Idaho-Oregon Real Field Co-deployment

The Earthscope IDOR project acquired geologic, geochemical, and geophysical data to investigate the tectonic evolution of accretion, transpression, and magmatism at the western margin of the North American craton (Tikoff et al., 2017). Broadband seismometers were used to collect teleseismic data (Stanciu et al., 2016; Bremner et al., 2019) and geophones were used to collect controlled-source seismic refraction and wide-angle reflection data (Davenport et al., 2017) to investigate subsurface crustal and upper mantle structure. Eighty-five broadband stations were deployed in a grid with 30-km spacing and along a line with 15-km spacing (Fig. 1). Controlled-source data were acquired by 2555 geophones at 200-m spacing along the same line (Fig. 1).

The broadband data were acquired by Guralp CMT-3T three-component seismometers with a 120-s natural frequency and Reftek RT130 dataloggers powered by two deep-cycle marine 12-V batteries with connected solar panels (Stanciu et al., 2016; Bremner et al., 2019). They were installed by experienced scientists, with a focus on data quality. The sites used were chosen to avoid flooding and high seismic noise areas, to be near bedrock for better coupling, to avoid vandalism and avoid sedimentary basins. More than one-person day was used to install each site, not including travel time. The stations recorded at 40 samples per second continuously from summer 2011 to summer 2013. Most stations recorded with quality comparable to the professionally installed Earthscope Transportable Array.

The controlled-source data were acquired using Geospace GS-11 single-component geophones with a 4.5 Hz natural frequency and Reftek RT125 "Texan" data-loggers powered by two 1.5 V D-cell alkaline batteries (Davenport et al., 2017). These are not modern industry "nodes" but are functionally equivalent stand-alone systems designed to be small, lightweight, and deployed in minutes. The disadvantage of this system is the 1990's electronics and batteries which limit recording time as compared to modern nodes. The 2555 stations were installed over 3 days across a large field area with long drive times. A large deployment crew was used, consisting of mostly undergraduate student volunteers with no field experience and a brief training. To facilitate rapid access and comply with permitting restrictions, stations were deployed along the roadside in loose sediment, with a few line segments along hiking trails. Many were near seismic noise sources, such as creeks and vehicle traffic. The geophones were stomped into the ground and buried a few centimeters deep.

For this study, a single broadband station within the Idaho Batholith and the adjacent geophone line were used (Figs. 1 & 2). The broadband station was buried in soil weathered in place near bedrock. The section of geophones used was within the edge of a creek valley with thin (probably <100 m) sediment, and about half of the stations were within 200 m of a creek. The broadband station was approximately 700 m from the nearest geophone, effectively co-located at a hard-rock site at frequencies well below 1 Hz. However, the distance and differences in soil or sediment will cause differences in signal at higher frequencies.

Signal Processing

All signal processing was performed using a the open-source Seismic Analysis Code (SAC) (Goldstein, 2003; Goldstein, 2005). The SAC scripts are provided in the Appendix for repeatability with these or other data. The geophone data were acquired and archived in 10-

minute time windows which were merged into daily windows similar to the broadband data. The geophone data were resampled from 250 to 50 samples per second, close to the 40 samples per second rate of the broadband seismograph.

A 30-minute window as chosen centered on each 10-minute window that would be used for analysis. Prior to any processing in the frequency domain, the data mean and trend were removed, a 9-minute cosine taper was applied to the ends of the 30-minute trace, and 150 minutes of zeroes were padded to the end of the trace. The broadband seismometer and geophones, were corrected for the seismometer and data-logger instrument response using the values in Table 1, converting the data to ground displacement in meters.

The mean and linear trend were again removed after the instrument correction. When a limited bandwidth was desired, an 8-pole Butterworth filter was applied. The time series were then cut to less than 10-minute windows for comparison. Power density spectra were computed from 10-minute traces tapered with a 0.5-minute taper and padded to 30 minutes with zeros using a fast Fourier transform, squaring the amplitude, and dividing by the trace length without padding (600 s). All comparisons were performed for the vertical component only, because 3-component geophone data were not acquired.

After instrument correction, the geophone ground displacement was a factor of ~50 larger than the broadband ground displacement at all frequencies. It was initially assumed that the instrument response parameters for the geophones were in error, as they are seldom used. However, the power density spectra indicated noise displacement on the broadband with amplitude smaller than the new low noise model (NLNM) for the vault stations (Peterson, 1993). This suggests that the error likely occurred in the instrument correction for the broadband instrument. The source of the error was not discovered. The broadband displacement data were

multiplied by a frequency-independent factor of 52. It is possible that this correction is incorrect, and all time-series amplitudes should be a factor of 52 smaller (power spectral density a factor of 2700 (52 squared) smaller); however, this correction does not have an impact on the conclusions of this study.

Sea of Okhotsk Teleseismic Event

A **M** 7.7 earthquake at approximately 580 km depth beneath the Sea of Okhotsk, near Poronaysk, Russia (Fig. 3) occurred on August 14, 2012 (Hayes et al., 2016) and was recorded on both the broadband seismometer and the geophones used for this study. Multiple, large-amplitude teleseismic arrivals from P and S paths through the mantle were recorded on both the broadband seismometer and the nearest geophone (Figs 4, 5, and 6). These arrivals were observed from the 20-Hz Nyquist frequency of the broadband data down to ~0.01 Hz (~100 s). Between ~0.03 Hz (32 s) and 1 Hz the waveforms are very similar for all arrivals. Below ~0.03 Hz the instrument noise from the geophone affects the signal and the waveforms are less similar. Above 1 Hz, the arrivals are observed on both instruments, but the scattered coda arrivals are different (Fig. 4). This is likely due to the 700-m distance between the instruments, thicker sediments at the geophone station and possibly differences in seismometer-soil coupling.

The ~15-km broadband station spacing and the ~200-m geophone spacing result in ~75 geophones per broadband station. Most nearby geophones recorded very similar data for the teleseism below 1 Hz, but higher noise is observed on a few of the geophones (Fig. 7). The densely spaced geophones allow the measurement of apparent velocity of each arrival. For example, the measured apparent velocity of the first P-wave arrival is 13.5 km/s.

The displacement power spectral density for the geophones is the same as the broadband seismometer down to <0.03 Hz (>32 s) and is very similar down to 0.02 Hz (50 s) (Fig. 8). At

lower frequencies (longer periods), the instrument self-noise begins to dominate the geophone signal and becomes larger than the ground shaking recorded by the broadband seismometer.

Ambient Noise

Major teleseismic events have large amplitude ground shaking at long periods that makes it easier to measure. The lowest amplitude seismic waves that are analyzed are ambient noise, which at longer periods are caused primarily by waves and storms in the ocean. The ambient-noise method uses cross-correlated noise on a pair of stations to produce a virtual source recorded on one of the instruments (Snieder, 2004). Random noise is correlated over very long time windows, typically months of data at ~0.1 Hz, to produce the desired signal.

The night before the teleseism occurred was a relatively quiet time period on both the broadband seismometer and the geophones. For short time windows (<10 min), the broadband seismometer and nearest geophone recorded similar waveforms down to ~0.25 Hz (4 s) (Figs. 9 and 10). The ambient noise on the geophone also differs from the broadband seismometer above 1 Hz. This is likely due to the 700-m distance between the geophone and broadband seismometers, thicker sediment at the geophone location, and the shallow burial of the geophone. The waveforms at 0.25 – 1 Hz are not identical, but are well correlated, and have a closely comparable shape and amplitude. The ambient-noise seismic method uses correlation over very long time windows. The broadband and geophone waveforms definitely correlate within this criterion.

The power spectral density of the geophone for a 10-minute noise window matches the broadband seismometer in shape down to ~0.15 Hz (7 s) (Fig. 10). This is at the low end of the microseism peak (Peterson, 1993). Although the broadband seismometer displacement was multiplied by a factor of 52 (and the power multiplied by ~2700) to match the geophone

response, the noise level of both seismometers compares well with the new low noise model (NLNM) (Peterson, 1993) (Fig. 10). The effective response of the geophone could be extended beyond 0.15 Hz using energy from longer time windows which are usually utilized for ambient noise studies, decreasing instrument self-noise by stacking over time. However, the ambient noise energy from 0.15 - 0.1 Hz (7 – 10 s) decreases as frequency decreases and differs greatly from the geophone self-noise as geophone self-noise increases in this frequency window. This may prevent much benefit from stacking in ambient noise.

Slant Stacking and Beam Forming of 77 Geophones

The additional geophone stations deployed between broadband stations offer the opportunity to improve signal through stacking. Instrument self-noise should differ at each geophone, so the signal to noise ratio should increase through stacking. Beam forming stacks data from stations at different locations as a function of the azimuth and the apparent velocity that the signal travels across the array. For the IDOR line segment that was chosen, the array was almost linear (Fig. 2). The back-azimuth of the incoming energy cannot be derived from a linear array, so the array was projected onto the known back azimuth of the Russian teleseism (Fig. 7). The data were then slant-stacked at different values of apparent slowness (inverse of velocity).

Stacking at an apparent P-wave velocity of 13.5 km/s, the stacked geophone data match the broadband and single geophone waveforms, but with slight amplitude differences (Fig. 12). This is likely due to using a stacking velocity to match the first P-wave arrival and not later arrivals. The power spectral density for this stacked trace matches the broadband station at lower frequencies, closer to 0.015 Hz (70 s) (Fig. 13), indicating that stacking improved the signal.

Most ambient noise energy is surface waves. In the granitic Idaho Batholith, the surface-wave velocity in the upper crust is ~3.5 km/s. Some surface wave noise will travel parallel to the linear array, but other surface waves will travel at different azimuths and appear as faster apparent velocities in the slant stack. The slant-stacked geophone ambient noise energy falls between -0.3 and +0.3 s/km slowness (~3.5 km/s velocity) (Fig. 14), consistent with surface waves, but not eliminating the possibility that body waves are recorded. The power spectral density for one of the slant-stacked traces is very similar to the single geophone (Fig. 15). It has a little lower power below ~0.15 Hz (7 s) than the single geophone, but because of the decrease in seismic energy at frequencies between 0.1 and 0.15 Hz, the match with the broadband seismometer is not significantly improved below 0.15 Hz.

Implications and Conclusions

Geophones like any other seismometer, can record signal well below their natural frequency (Rodgers, 1994; Chapman, 2009). An instrument correction must be applied, and the decrease in instrument sensitivity at lower frequencies results in a loss of effectiveness at lower frequencies. At sufficiently low frequency, instrument self-noise will exceed the ability to record ground motion, but the boundary of that effectiveness depends on the magnitude of the ground motion.

This study compares nearby geophones and broadband seismometers realistically deployed as part of geologically motivated arrays. The instruments were not deployed for direct comparison. The broadband seismometers were deployed careful by experienced scientists, but under normal field project conditions that are worse than a typical vault. The geophones were deployed much more rapidly and in poorer field conditions than the broadband seismometers.

For a large magnitude teleseism, geophones recorded the same seismic signal as broadband seismometers down to 0.02-0.03 Hz (32-50 s) (Figs. 4-6 and 8). Low energy, ambient noise was recorded successfully down to 0.15-0.25 Hz (4-7 s) (Figs. 9-11). Despite field conditions that were less than ideal, the geophones recorded quality signal more than 1-2 orders of magnitude (depending on the source) below their natural frequency.

The field observations of ambient noise in this study are consistent with calculated self-noise spectra. These spectra indicate that the self-noise of 1-2 Hz passive electromagnetic sensors is at or below the NLNM (Peterson, 1993) down to 0.1-0.2 Hz (5-10 s) (Rodgers, 1994). The computed self-noise spectrum of a 4.5-Hz geophone was not far above the NLNM. Similar results were obtained recording real seismic data in a permanent vault with a passive 1-Hz seismometer acquiring high-quality signal to ~0.1 Hz (~10 s) (Chapman, 2009). While results do depend upon the sensor and amplifier (Rodgers, 1994), they primarily shift in frequency proportional to the natural frequency of the seismometers. The lowest frequency with quality signal is similar in this study as well as cited studies. The lowest frequency with good signal is controlled by growing instrument self-noise as frequency decreases. This self-noise approaches and then rapidly exceeds seismic noise below 0.1-0.2 Hz (5-10 s) in ambient noise environments in part because the ambient noise decreases in amplitude from ~0.15 to ~0.02 Hz (7-50 s). The instrument self-noise and seismic noise diverge greatly in this frequency range for ambient noise environments. This study shows that realistic field conditions have less of an effect on effectiveness at these ranges than the instrument self-noise. The minimum frequency with high-quality ambient noise signal from 1-5 Hz passive seismometers is 0.1-0.2 Hz (5-10 s). Larger seismic signals can be recorded at even lower frequencies (longer periods).

Long-period broadband seismometers are the best sensors at periods of tens to hundreds of seconds. However, due to cost, weight, power demands, and field effort, broadband seismometers cannot be deployed at dense enough spacing to eliminate spatial aliasing at frequencies above roughly 0.1 Hz (periods less than 10 s). Geophone nodes, by comparison, are much less expensive and lighter, require less power, and can be deployed more rapidly. By using arrays of low-frequency geophones down to their full potential which is 5 – 10 s for ambient seismic energy and >50 s for large magnitude teleseismic events, spatial aliasing could be alleviated. A combination of broadband and geophone sensors in a deployment, optimizing the spatial sampling and instrument sensitivity of each, could record broadband full seismic wavefields rather than spatially aliased wavefields.

There are many applications in seismology that fall within the practical, effective range of geophones from roughly 0.1 to 10 Hz. Earthquakes damage buildings, volcanic magma migration produces ground shaking, and large explosive sources produce far-field signals within this bandwidth. Most teleseismic receiver function studies of the lithosphere and ambient-noise studies of the crust also fall within this bandwidth and are usually spatially aliased. Increasing station density is essential to focus on these scientific targets, improving spatial resolution by enabling full-wavefield imaging methods. Arrays of geophone nodes embedded between broadband seismometers can bridge this gap.

References Cited

Al-Eqabi, G. I., Koper, K. D., and Wysession, M. (2001). Source Characterization of Nevada Test Site Explosions and Western U.S. Earthquakes using Lg Waves: Implications for Regional Source Discrimination, *Bull. Seismol. Soc. Am.,* ***91,*** *140-153.*

Almendros, J., Chouet, B., Dawson, P., and Bond, T. (2001). Identifying elements of the plumbing system beneath Kilauea Volcano, Hawaii, from the source locations of very-long-period signals, *Geophys. J. Int.* **148,** 303-312.

Bormann, P. (1993). Conversion and comparability of data presentations on seismic background noise, *J. of Seismol.* **2,** 37-45.

Bremner, P. M., Panning, M. P., Russo, R. M., Mocanu, V., Stanciu, A. C., Torpey, M., Hongsresawat, S., VanDecar, J. C., LaMaskin, T. A., and Foster, D. A. (2019). Crustal shear wave velocity structure of central Idaho and eastern Oregon from ambient seismic noise: Results from the IDOR project, *J.Geophys. Res. Solid Earth* **124**, 1-25, doi:10.1029/2018JB016350

Brenguier, F., Kowalski, P., Ackerley, N., Nakata, N. Boué, P., Campillo, M., Larose, E., Rambaud, S., Pequegnat, C., Lecocq, T., Roux, P., Ferrazzini, V., Villeneuve, N., Shapiro, N. M., and Chaput, J. (2016). Toward 4D Noise-Based Seismic Probing of Volcanoes: Perspectives from a Large-N Experiment on Piton de la Fournaise Volcano, *Seismol. Res. Lett.* **87,** no. 1, 15-25, doi:10.1785/0220130173.

Chapman, M., 2009, A comparison of Short-Period and Broadband Seismograph Systems in the Context of the Seismology of the Eastern United States: Seismological Research Letters, v. 80, p. 1019-1034, doi:10.1785/gssrl.80.6.1019

Davenport, K. K., Hole, J. A., Quiros, D. A., Brown, L. D., Chapman, M. C., Han, L., and Mooney, W. D., 2015, Aftershock imaginig using a dense seismometer array (AIDA) after the 2011 Mineral, Virginia, earthquake: *In* Horton, J. W., Jr., Chapman, M. C., and Green, R. A., eds., The 2011 Mineral Virginia, Earthquake, and Its Significance for Seismic Hazards in Easter North America: *Geol. Soc. Amer. Special Paper* **509,** p. 273-283. Doi:10.1130/2015.2509(15)

Davenport, K.K., Hole, J.A., Tikoff, B., Russo, R.M., and Harder, S.H. (2017). A Strong Contrast in Crustal Architecture from Accreted Terranes to Craton, Constrained by Controlled-Source Seismic Data in Idaho and Eastern Oregon, *Lithosphere* **9,** no. 2, 325-340, doi:10.1002/2016JB012989.

Gallipoli, M. R., Mucciarelli, M., Sket-Motnikar, B., Zupancic, P., Gosar, A., Prevolnik, S., Herak, M., Stipcevic, J., Herak, D., Milutinovic, Z., and Olumceva, T. (2010) Empirical estimates of dynamic parameters on a large set of European buildings, *Bull. Earthquake Eng.* **8,** 593-607, doi:10.1007/s10518-009-91233-6.

Glasgow, M. E., Schmandt, B. and Hansen, S. M. (2018). Upper crustal low frequency seismicity at Mount St. Helens detected with a dense geophone array, *J. Volcanol. Geotherm. Res.* **358,** 329-341. doi:10.1016/j.jvolgeores.2018.06.006

Goldstein, P., Snoke, A. (2005). "SAC Availability for the IRIS Community", Incorporated Institutions for Seismology Data Management Center Electronic Newsletter.

Goldstein, P., Dodge, D., Firpo, M., and Minner, L. (2003). "SAC2000: Signal processing and analysis tools for seismologists and engineers, Invited contribution to "The IASPEI International Handbook of Earthquake and Engineering Seismology", Edited by WHK Lee, H. Kanamori, P.C. Jennings, and C. Kisslinger, Academic Press, London.

Hansen, S. M. and Schmandt, B. (2015). Automated detection and location of microseismicity at Mount St. Helens with a large-N geophone array, *Geophys. Res. Lett.* **42**, 7390-7397, doi:10.1002/2015GL064848

Hayes, G. P., Myers, E. K., Dewey, J. W., Briggs, R. W., Earle, P. S., Benz, H. M., Smocyzk, G. M., Flamme, H. E., Barnhart, W. D., Gold, R. D., and Furlong, K. P. (2016) Tectonic Summaries of Magnitude 7 and Greater Earthqakes from 2000 to 2015, U.S. Geological Survey, Open-file report 2016-1192, p. 101.

Hong, L. L. and Hwang, W. L. (2000). Empirical formula for fundamental vibration periods of reinforced concrete buildings in Taiwan, *Earthquake Eng. Struct. Dyn.* **29,** 327-337.

Karplus, M. and Schmandt, B. (2018). Preface to the Focus Section on Geophone Array Seismology, *Seismol. Res. Lett.* **89,** no. 5, 1597-1600, doi:10.1785/0220180212.

Lin F. C., Li D., Clayton, R. W., and Hollis, D (2013). High-resolution 3D shallow crustal structure in Long Beach, California: Application of ambient noise tomography on a dense seismic array, *Geophysics* **78**, no. 4, Q45-Q56, doi:10.1190/GEO2012-0453.1.

Liu, G., Persaud, P. and Clayton R. W. (2018). Structure of the Northern Los Angeles Basins Revealed in Teleseismic Receiver Functions from Short-Term Nodal Seismic Arrays, *Seismol. Res. Lett.* **89,** no. 5, 1680-1689, doi:10.1785/0220180071.

Peterson, J. (1993). Observations and Modeling of Background Seismic Noise, U.S. Geological Survey, Open-file report 93-322, 94p.

Ranasinghe, N. R., Worthington, L. L., Jiang, C., Schmandt, B., Finlay, T. S., Bilek, S. L., and Aster, R.C. (2018). Upper-Crustal Shear-Wave Velocity Structure of the South-Central Rio Grande Rift above the Socorro Magma Body Imaged with Ambient Noise by the Large-N Sevilleta Seismic Array, *Seismol. Res. Lett.* **89,** no. 5, 1708-1719, doi:10.1785/0220180074.

Rodgers, P.W. (1994). Self-Noise Spectra for 34 Common Electromagnetic Seismometer/Preamplifier Pairs: *Bull. Seismol. Soc. Am.*, **84,** 222-228.

Snieder, R. (2004). Extracting the Green's function from the correlation of coda waves: A derivation based on stationary phase, *Physical* **69,** 046610, 1-8.

Snieder, R. and Safak, E. (2006). Extracting the Building Response Using Seismic Interferometry: Theory and Application to the Millikan Library in Pasadena, California, *Bull. Seismol. Soc. Am.* **96,** no. 2, 586-598, doi:10.1785/0120050109.

Stanciu, A. C., Russo, R. M., Mocanu, V. I., Bremner, P. M., Hongsresawat, S., Torpey, M. E., VanDecar, J. C., Foster, D. A., and Hole, J. A. (2016). Crustal Structure Beneath the Blue Mountains Terranes and Cratonic North America, Eastern Oregon and Idaho, from Teleseismic Receiver Functions, *J. Geophys. Res. Solid Earth* **121,** 5049-5067, doi:10.1002/2016JB012989.

Tikoff, B., Vervoort, J., Hole, J. A., Russo, R., Gaschnig, R., and Fayon, A. (2017). Introduction: EarthScope IDOR project (deformation and magmatic modification of a steep continental margin, western Idaho–eastern Oregon) themed issue, *Lithosphere* **9,** no. 2, 151-156, doi:10.1130/L628.1.

Trow, A. J., Zhang, H., Record, A. S., Mendoza, K. A., Pankow, K. L., and Wannamaker, P. E. (2018) Microseismic Event Detection Using Multiple Geophone Arrays in Southwestern Utah, *Seismol. Res. Lett.* **89,** no. 5, 1660-1670, doi:10.1785/0220180065.

Wang, Y., Lin, F. C., Schmandt, B., and Farrell, J. (2017). Ambient noise tomography across Mount St. Helens using a dense seismic array, *J. Geophys. Res. Solid Earth* **122,** 1-17, doi:10.1002/2016JB013769.

Table 1

Broadband Poles and Zeros		**Geophone Poles and Zeros**	
Zeros	**2**	**Zeros**	**2**
+0.00e+00	+0.00e+00	+0.00e+00	+0.00e+00
+0.00e+00	+0.00e+00	+0.00e+00	+0.00e+00
Poles	**5**	**Poles**	**2**
-3.70e-02	+3.70e-02	-0.1979e+02	+0.2019e+02
-3.70e-02	-3.70e-02	-0.1979e+02	-0.2019e+02
-5.03e+02	+0.00e+00	**Constant**	1.634
-1.01e+03	+0.00e+00		
-1.13e+03	+0.00e+00		
Constant	+5.409061e+17		

List of Figures:

Figure 12. Same as Fig. 6, adding a slant stacked trace using a stacking velocity of 13.5 kms to match the P-wave arrival.

Figure 13. Same as Fig. 8, adding the power spectral density of the slant stacked trace from Fig. 12.

Figure 14. Slant stack of the 77 geophones in green in Fig. 2 for a 10-minue quiet ambient noise window recorded on August 13, 2012. Stacked at several slowness values from -0.5 s/km to 0.5 s/km using a west-to-east azimuth relative to the central station. -0.3 s/km represents surface waves moving ~3.5 km/s to the west. 0.3 s/km represents surface waves moving ~3.5 km/s to the east. Zero s/km represents surface waves moving perpendicular to the line.

Figure 15. Same as Fig. 11, adding the power spectral density of one slant stacked trace from Fig. 14.

Figure 1

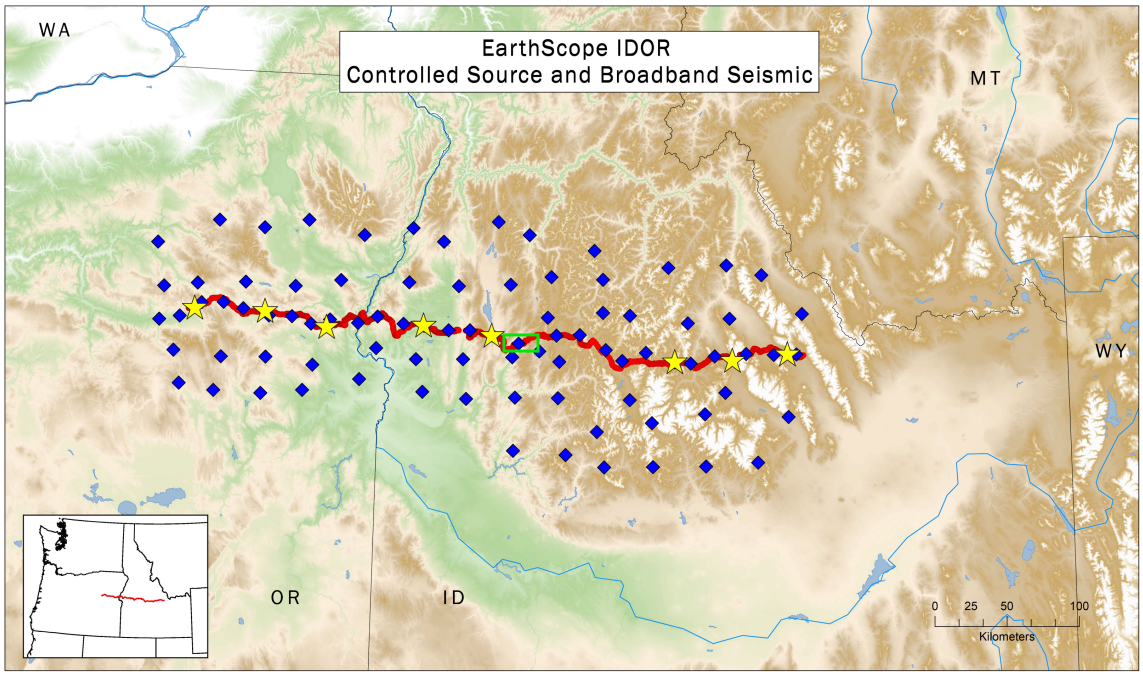
WA
EarthScope IDOR
Controlled Source and Broadband Seismic
MT
WY
OR
ID
0 25 50 100
Kilometers

Figure 2

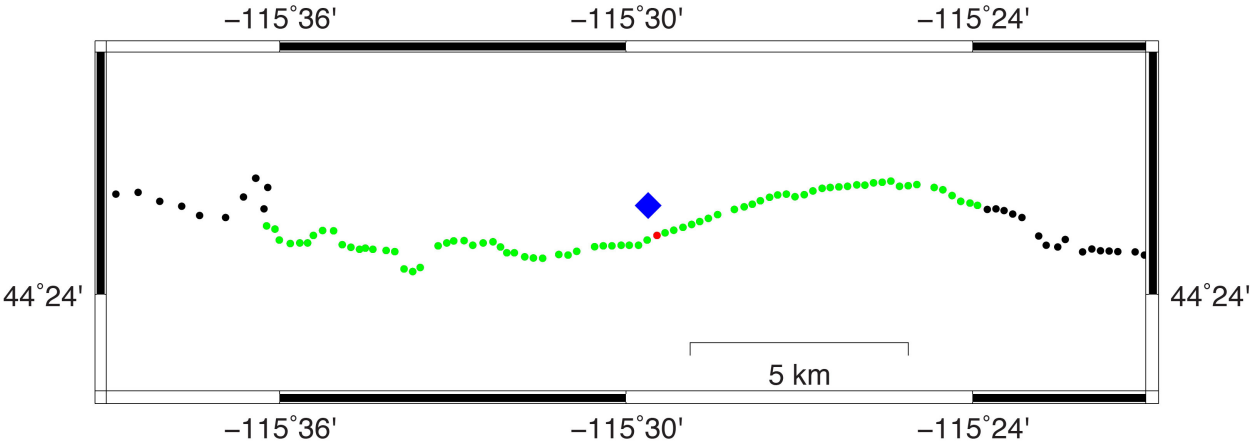

Figure 3

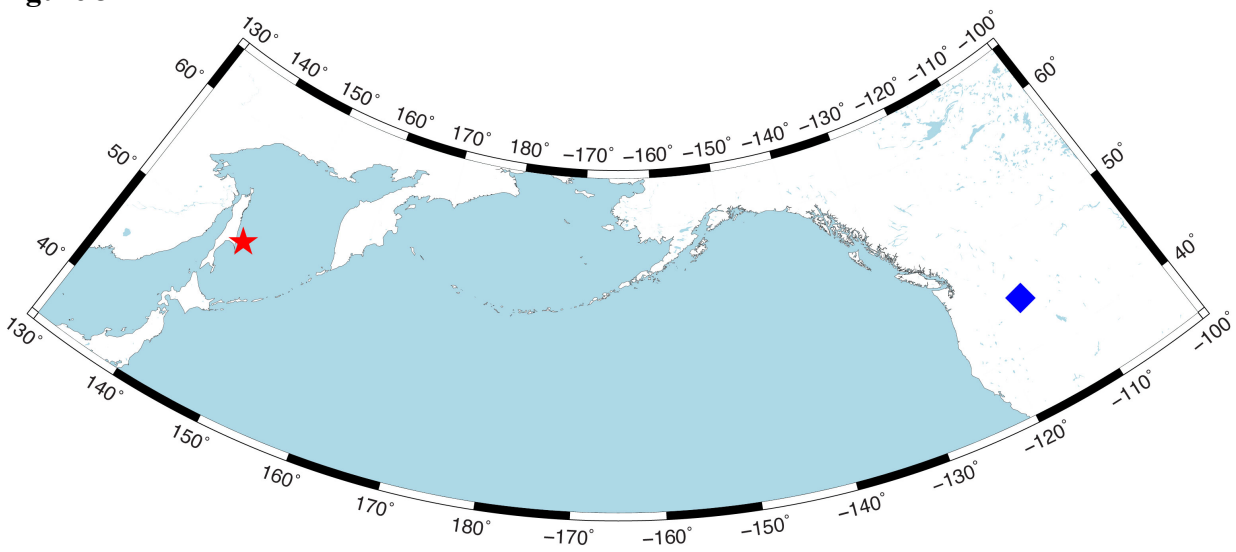

Figure 4

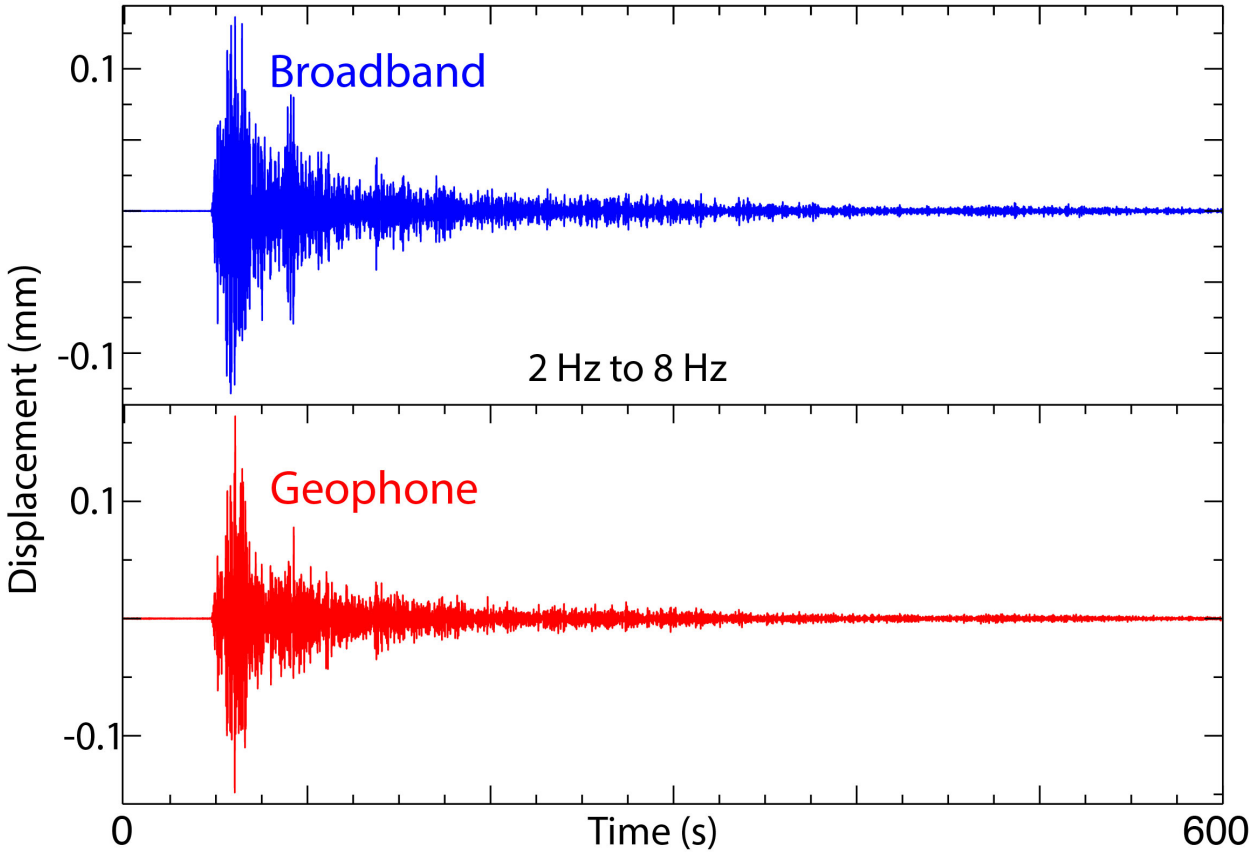
Broadband
2 Hz to 8 Hz
Geophone
0.1
-0.1
0.1
-0.1
Displacement (mm)
0
Time (s)
600

Figure 5

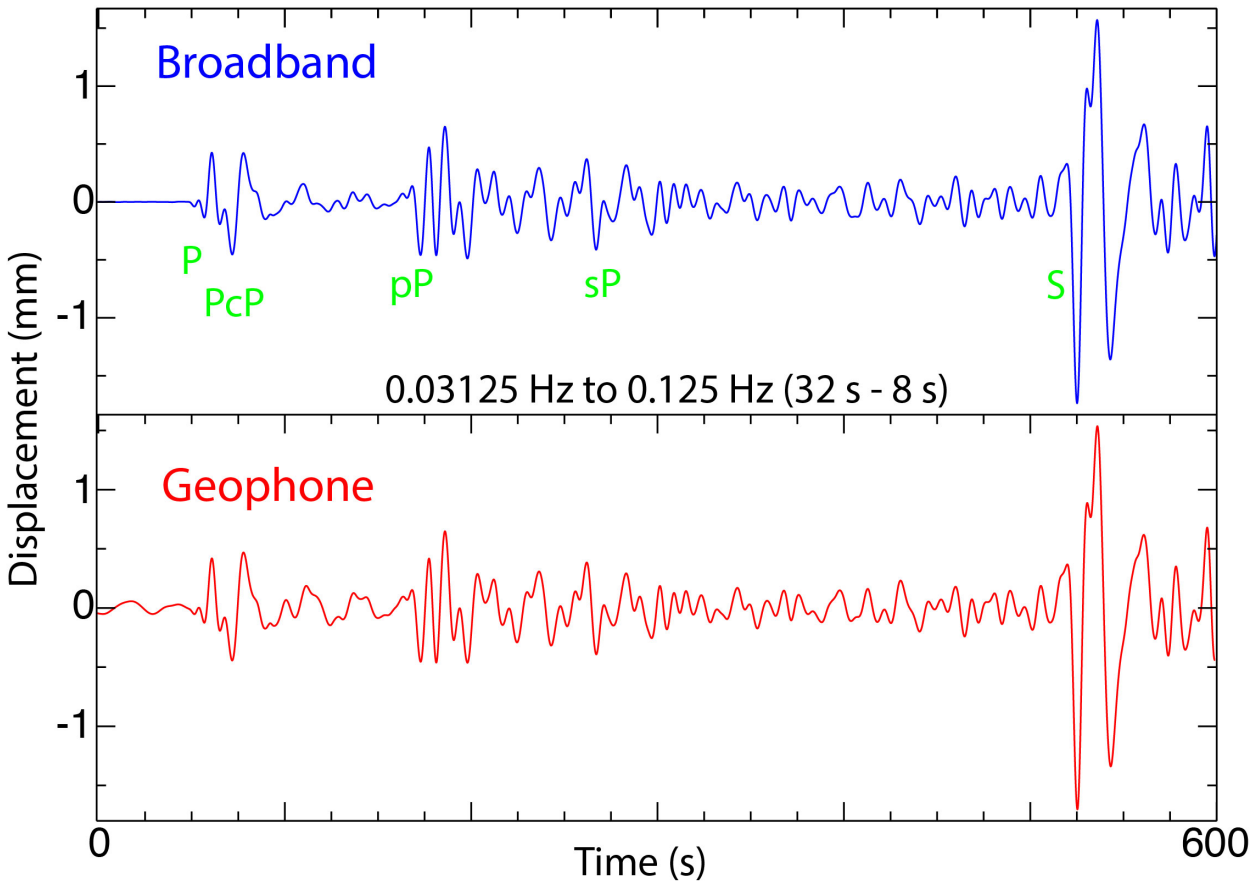
Broadband
Geophone
P
PcP
pP
sP
S
0.03125 Hz to 0.125 Hz (32 s - 8 s)
Displacement (mm)
1
0
-1
0
600
Time (s)

Figure 6

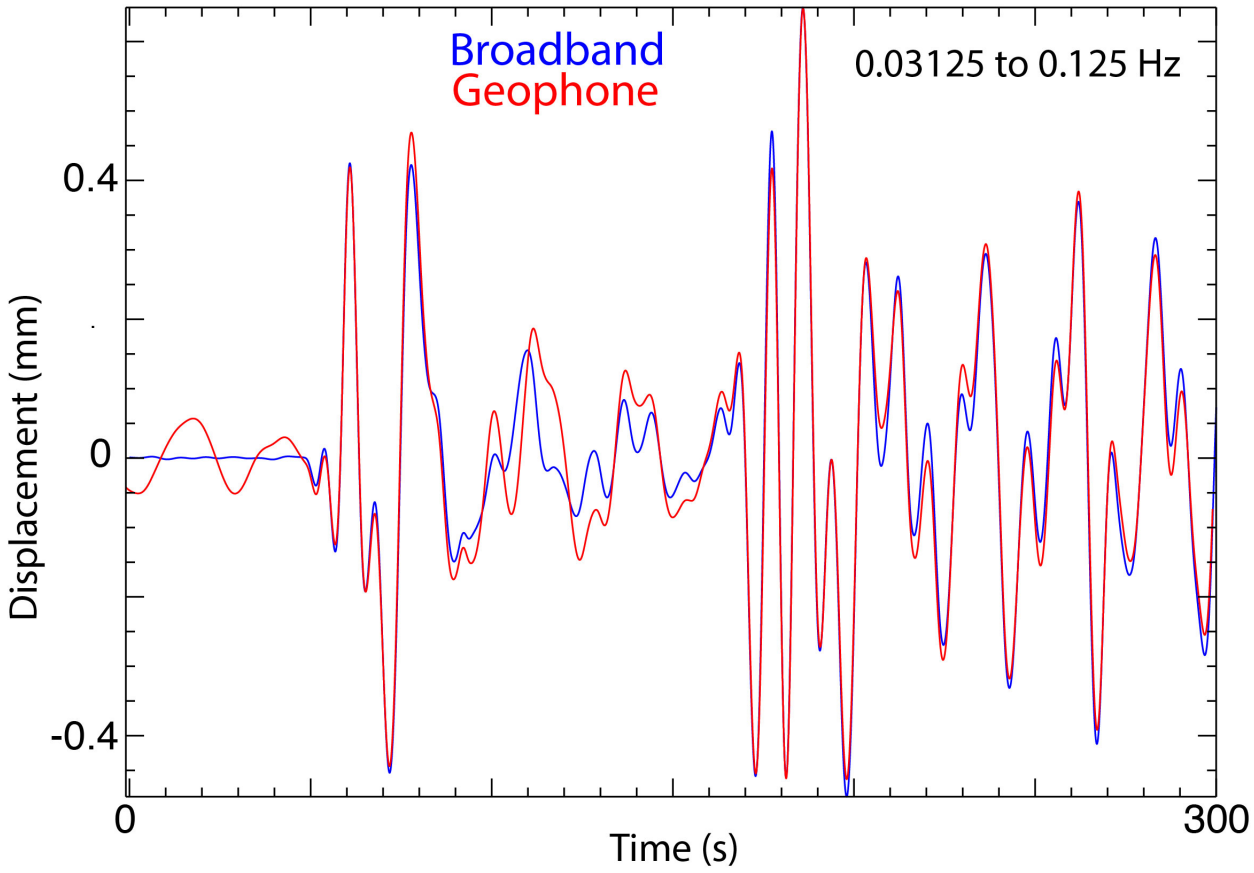
Broadband
Geophone
0.03125 to 0.125 Hz
0.4
0
-0.4
Displacement (mm)
0
300
Time (s)

Figure 7

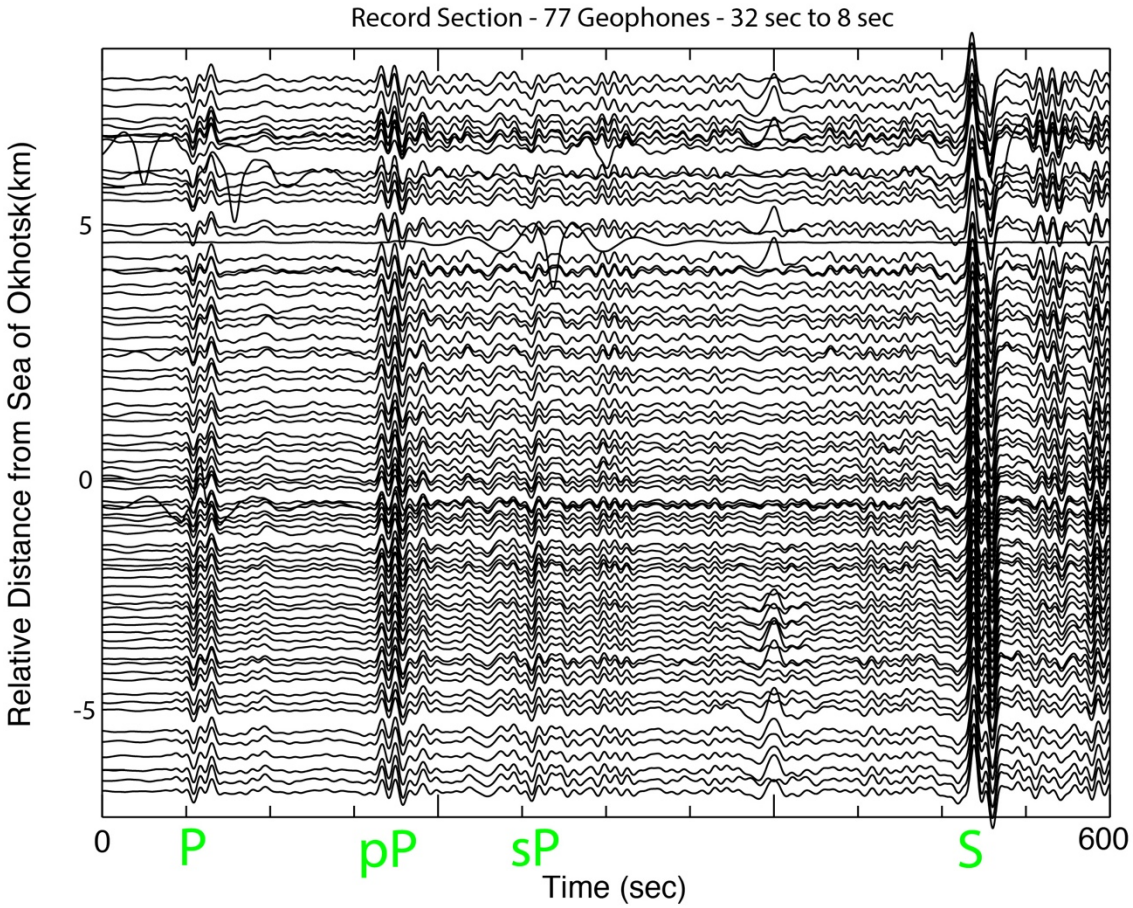
Record Section - 77 Geophones - 32 sec to 8 sec
Relative Distance from Sea of Okhotsk(km)
5
0
-5
0
P
pP
sP
S
600
Time (sec)

Figure 8

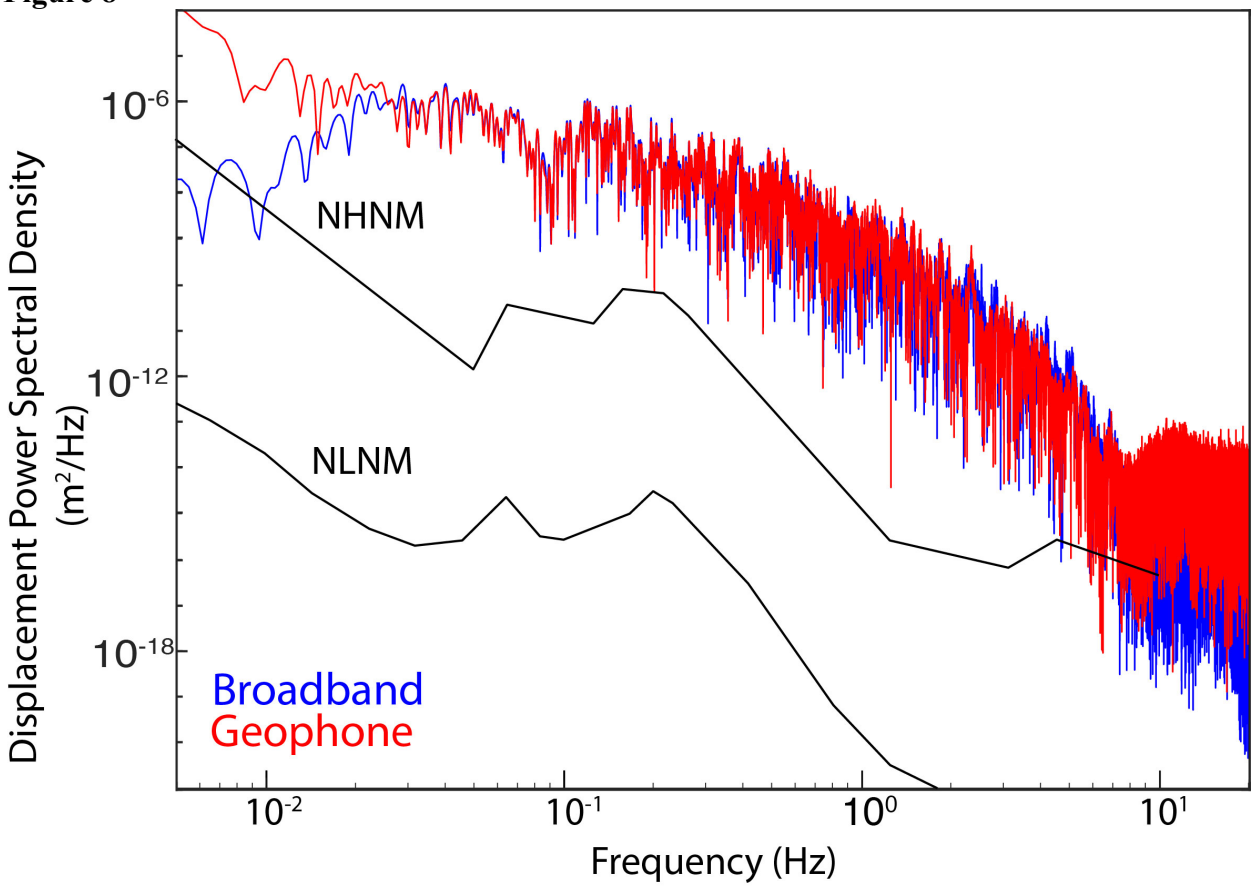
Displacement Power Spectral Density
(m²/Hz)
10-6
10-12
10-18
NHNM
NLNM
Broadband
Geophone
10-2
10-1
100
101
Frequency (Hz)

Figure 9

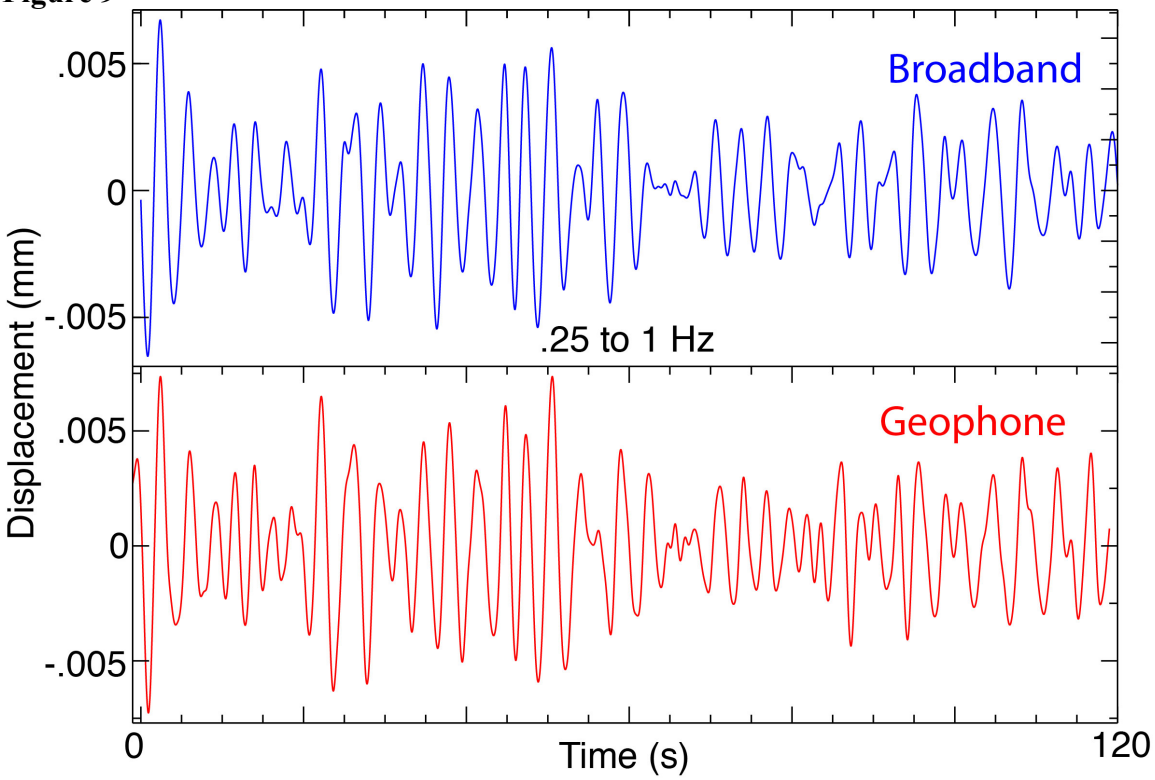
.005
0
-.005
Broadband
.25 to 1 Hz
.005
0
-.005
Geophone
Displacement (mm)
0
Time (s)
120

Figure 10

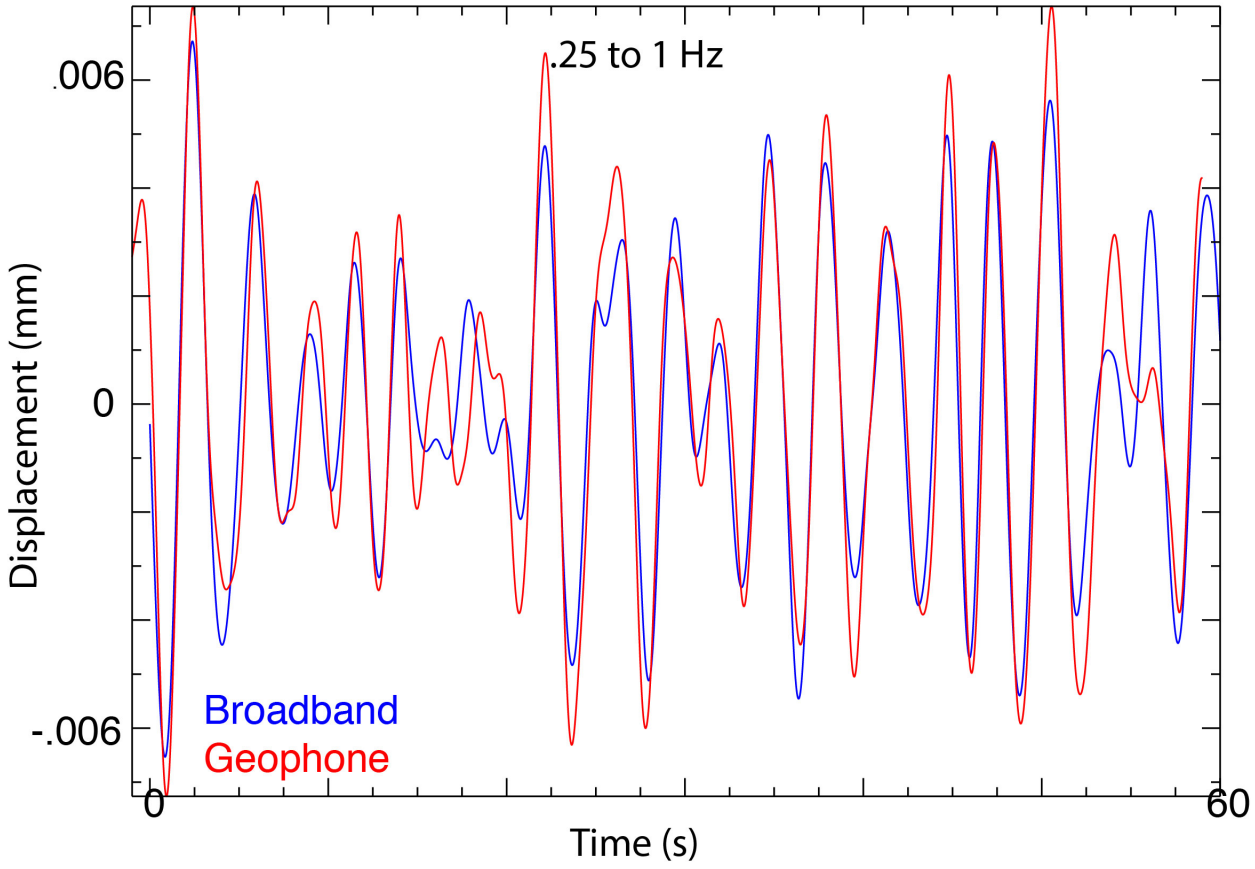
.25 to 1 Hz
.006
0
-.006
Displacement (mm)
Broadband
Geophone
0
60
Time (s)

Figure 11

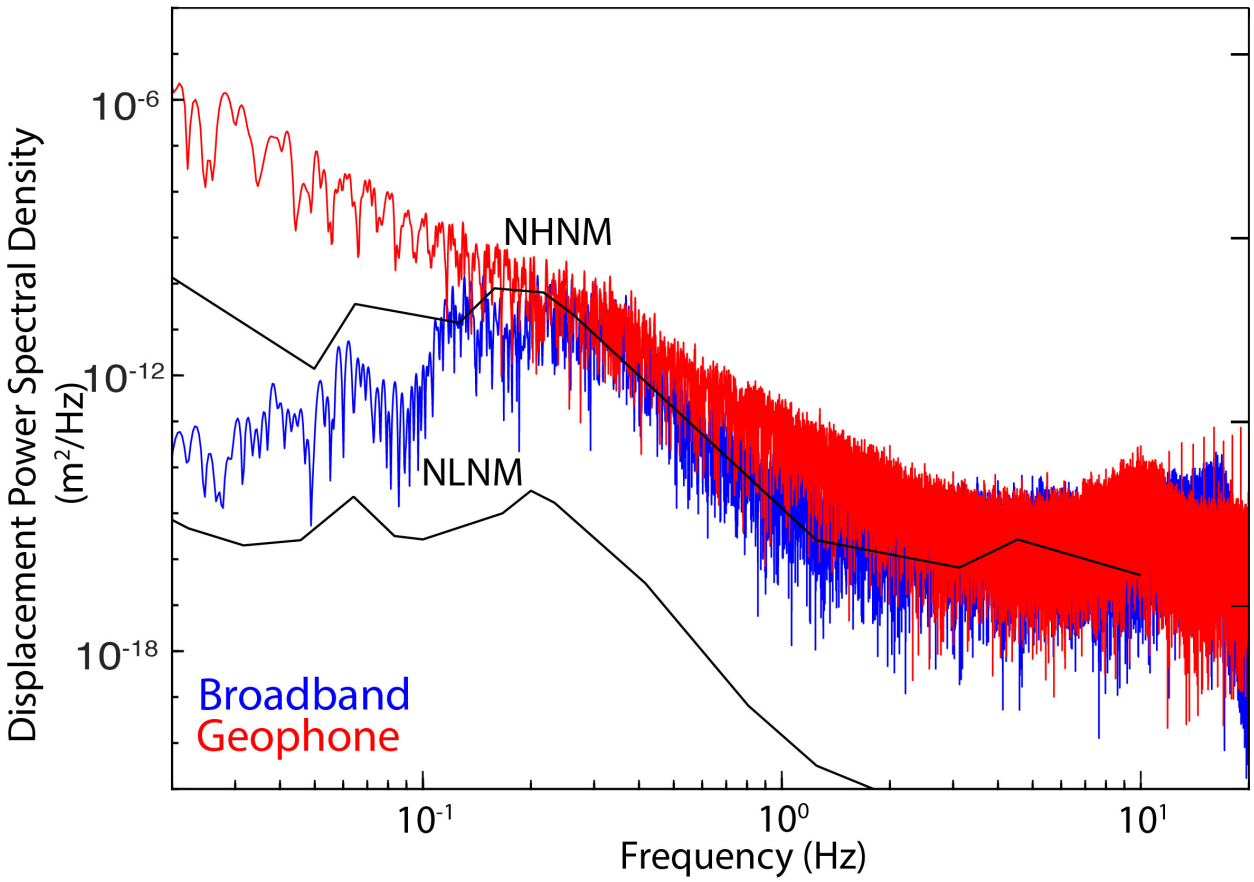
Displacement Power Spectral Density
(m²/Hz)
10⁻⁶
10⁻¹²
10⁻¹⁸
NHNM
NLNM
Broadband
Geophone
10⁻¹
10⁰
10¹
Frequency (Hz)

Figure 12

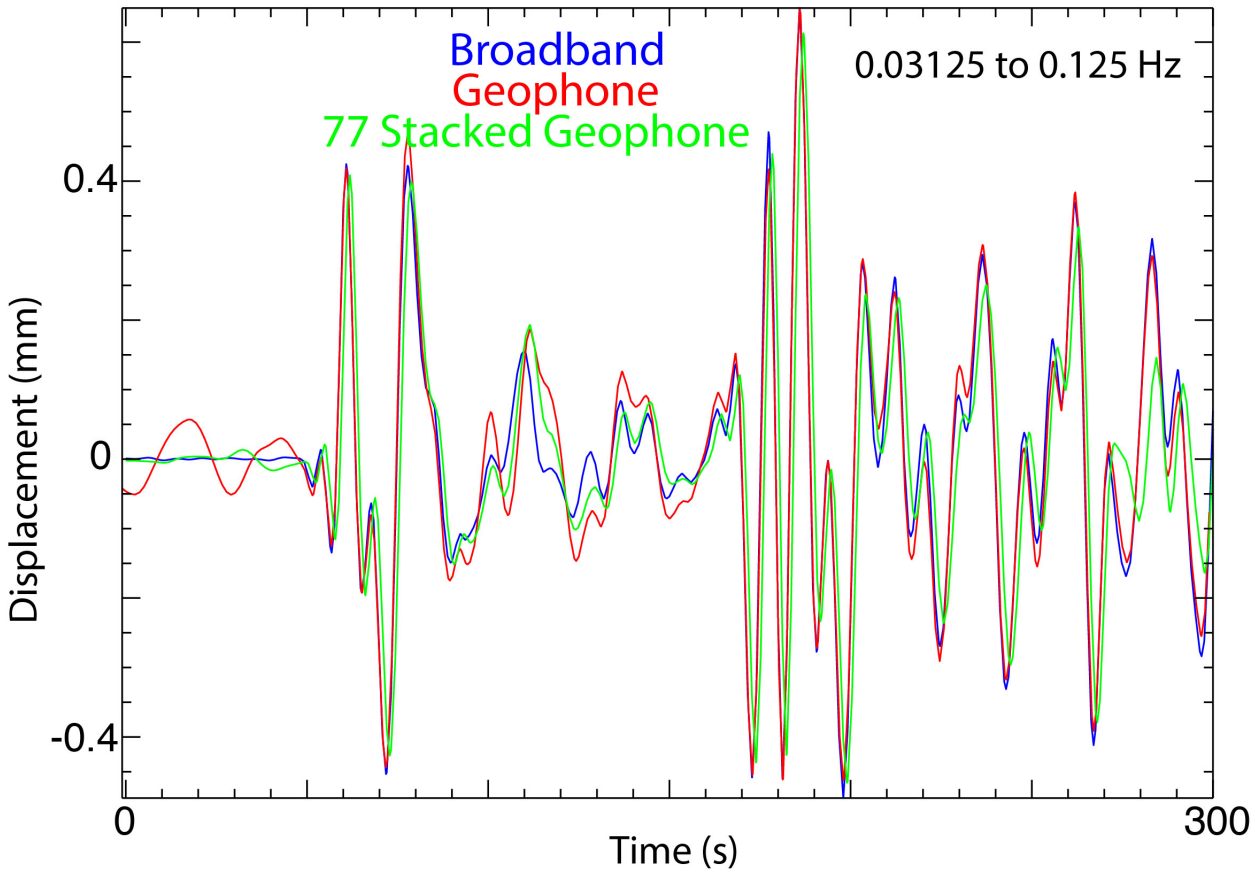
Broadband
Geophone
77 Stacked Geophone
0.03125 to 0.125 Hz
0.4
0
-0.4
Displacement (mm)
0
300
Time (s)

Figure 13

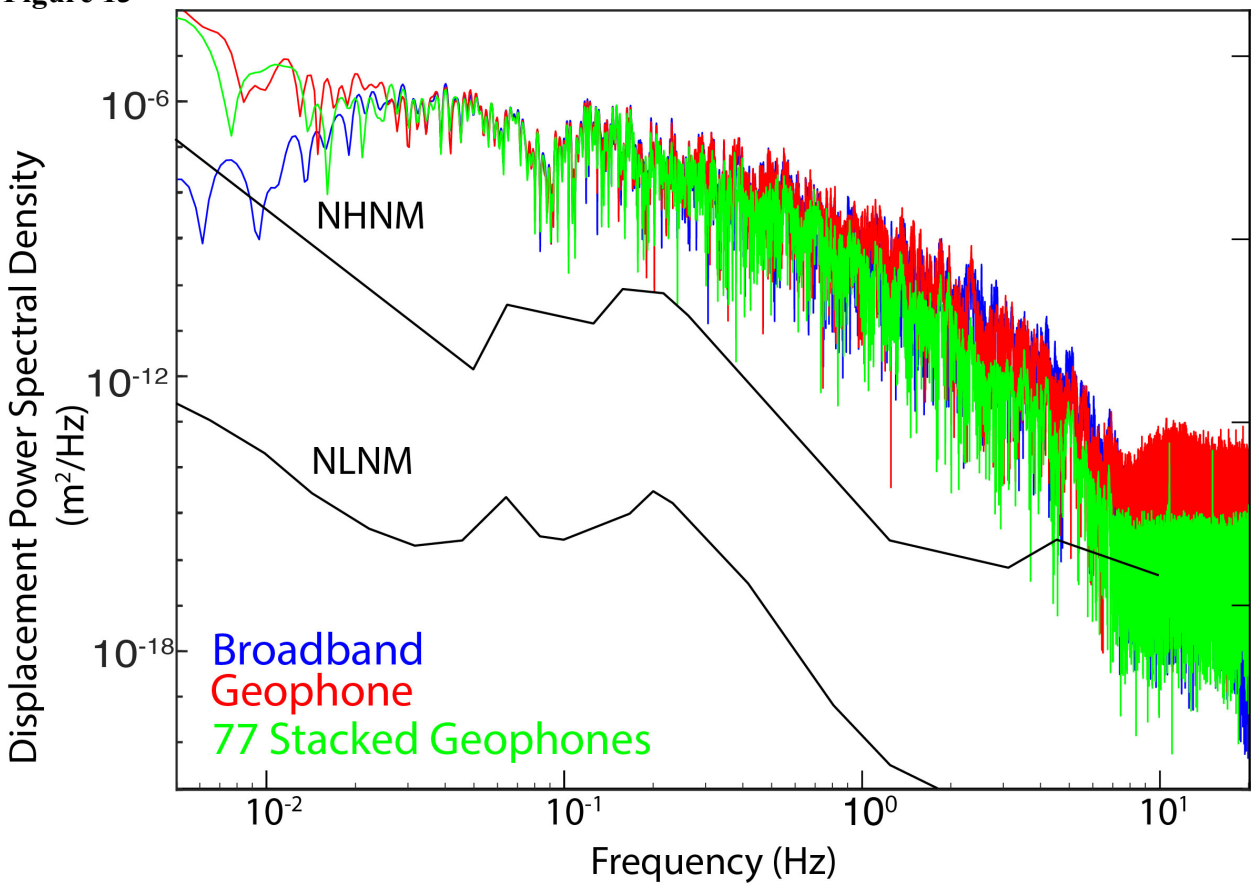
Displacement Power Spectral Density (m²/Hz)
10-6
10-12
10-18
NHNM
NLNM
Broadband
Geophone
77 Stacked Geophones
10-2
10-1
100
101
Frequency (Hz)

Figure 14

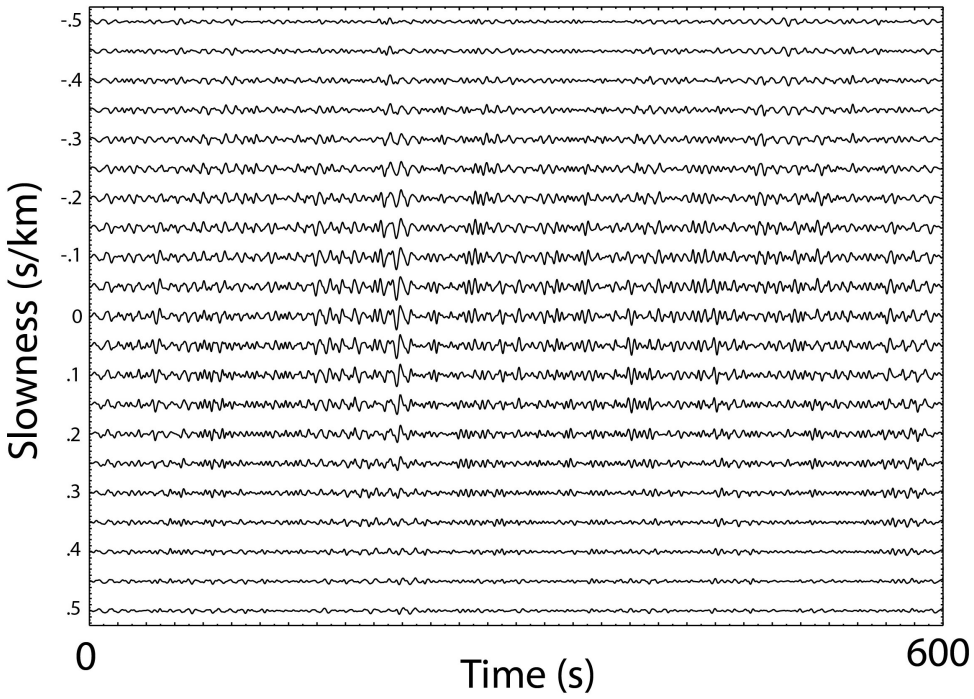

Figure 15

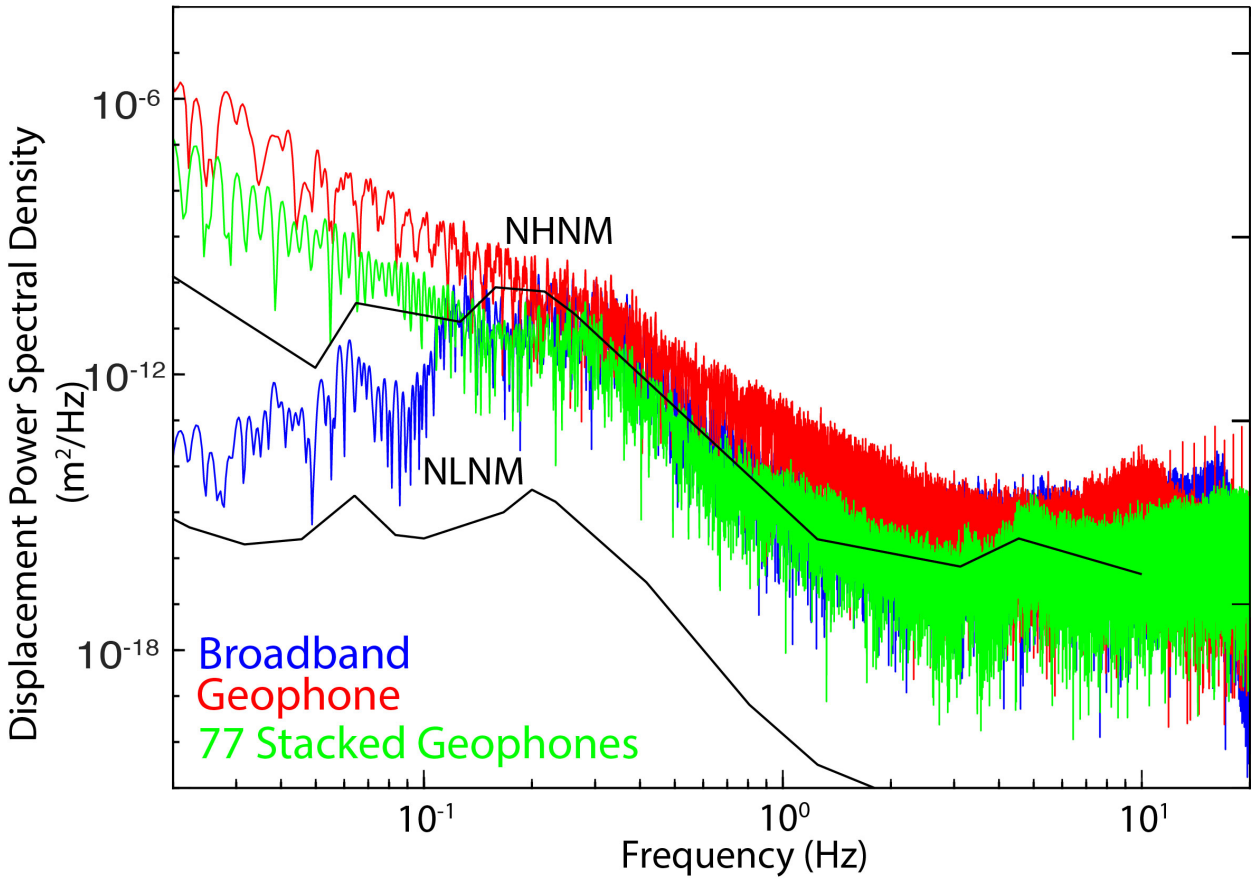
Displacement Power Spectral Density (m²/Hz)
10-6
10-12
10-18
NHNM
NLNM
Broadband
Geophone
77 Stacked Geophones
10-1
100
101
Frequency (Hz)

Appendix
SAC Scripts

Representative scripts using the Seismic Analysis Code (Goldstein, 2003, Goldstein, 2005) version 101.6a.

For variables that differ between the teleseism and the ambient noise window, the values for the teleseism are shown.

#1: Merge geophone 10-minute windows

```
DO station LIST 14062 12928 14016 14072 13678 13990 13989 13616
14026 13592 14014 14030 14061 12880 13788 13609 13837 13770
13854 13874 13650 13907 14076 13507 13676 13945 13947 12537
13663 12550 12508 12590 12551 12993 12902 12506 13844 12881
13620 13768 12509 13608 13991 13971 13884 13787 12591 13850
12922 13716 12539 12757 12583 14053 14009 13979 12572 13718
13955 13891 13826 13859 13863 12869 13664 12981 14095 13838
14038 12896 14006 12920 13638 13936 14071 12837 13622 13916

*Reads in all files during any continuous collection window.
SAC will have round off errors for non-continuously recorded
samples
READ IDOR_2012_227_00_*_00.000_$station$_Z_00001.SAC
IDOR_2012_227_01_*_00.000_$station$_Z_00001.SAC
IDOR_2012_227_02_*_00.000_$station$_Z_00001.SAC
IDOR_2012_227_03_*_00.000_$station$_Z_00001.SAC
IDOR_2012_227_04_*_00.000_$station$_Z_00001.SAC
IDOR_2012_227_05_*_00.000_$station$_Z_00001.SAC
IDOR_2012_227_06_*_00.000_$station$_Z_00001.SAC
IDOR_2012_227_07_*_00.000_$station$_Z_00001.SAC
IDOR_2012_227_08_*_00.000_$station$_Z_00001.SAC
IDOR_2012_227_09_*_00.000_$station$_Z_00001.SAC
IDOR_2012_227_10_*_00.000_$station$_Z_00001.SAC
IDOR_2012_227_11_*_00.000_$station$_Z_00001.SAC

merge verbose
write ../227_merge/IDOR_2012_227_00-11_$station$.SAC

READ IDOR_2012_227_17_*_00.000_$station$_Z_00001.SAC
IDOR_2012_227_18_*_00.000_$station$_Z_00001.SAC
IDOR_2012_227_19_*_00.000_$station$_Z_00001.SAC
IDOR_2012_227_20_*_00.000_$station$_Z_00001.SAC
IDOR_2012_227_21_*_00.000_$station$_Z_00001.SAC
IDOR_2012_227_22_*_00.000_$station$_Z_00001.SAC
IDOR_2012_227_23_*_00.000_$station$_Z_00001.SAC
```

```
merge verbose
write ../227_merge/IDOR_2012_227_17-23_$station$.SAC

ENDDO
```

#2: Resample geophone data

```
DO station LIST 14062 12928 14016 14072 13678 13990 13989 13616
14026 13592 14014 14030 14061 12880 13788 13609 13837 13770
13854 13650 13907 14076 13507 13676 13945 13947 12537 13663
12550 12508 12590 12551 12993 12902 12506 13844 12881 13620
13768 12509 13608 13991 13971 13884 13787 12591 13850 12922
13716 12539 12757 12583 14053 14009 13979 12572 13718 13955
13891 13826 13859 13863 12869 13664 12981 14095 13838 14038
12896 14006 12920 13638 13936 14071 12837 13622 13916

read R226/226_merge/IDOR_2012_226_04-11_$station$.SAC

DECIMATE 5

write R226/resample/IDOR_2012_226_04-11_$station$.SAC

read R226/226_merge/IDOR_2012_226_17-23_$station$.SAC

DECIMATE 5

write R226/resample/IDOR_2012_226_17-23_$station$.SAC

read R227/227_merge/IDOR_2012_227_00-11_$station$.SAC

DECIMATE 5

write R227/resample/IDOR_2012_227_00-11_$station$.SAC

read R227/227_merge/IDOR_2012_227_17-23_$station$.SAC

DECIMATE 5

write R227/resample/IDOR_2012_227_17-23_$station$.SAC

read R228/228_merge/IDOR_2012_228_00-11_$station$.SAC

DECIMATE 5

write R228/resample/IDOR_2012_228_00-11_$station$.SAC

ENDDO
```

#3: Perform Instrument Response Corrections

```
*This script is used to do the processing before the transfer
*function
*Individual variables can be set using the setbb command and can
*be changed to desired values.
*Variables can be defined as strings with spaces or values, but
*are limited to 32 characters.

*Files to be read in
setbb GEOPHONE IDOR_2012_227_00-11_13991.SAC
setbb BROADBAND 2012.227.L11.BHZ.M.SAC

*Values selected to adjust the time window to the desired 30
minute window
setbb TIME1GP 10400
setbb TIME2GP 12200
setbb TIME1BB 10700
setbb TIME2BB 12500

*PoleZero File for instrument corrections for geophones and
*broadbands
setbb GPPZ ../GP_IR_2_ZEROS
setbb BBPZ ../IDOR_PZs_XT.L11.BHZ

*Frequency values for the transfer function
setbb f2 .005
evaluate to f1 %f2 / 1.5
setbb f3 100
setbb f4 150


*Colors and defaults that effect the processing are turned off
color off
xlim off
ylim off
linlin
qdp off

*Files to Write
setbb BBWRITE Transfer.Broadband.SAC
setbb GPWRITE Transfer.Geophone.SAC

*Geophone processing to transfer function
r %GEOPHONE
cutim %TIME1GP %TIME2GP
rmean
rtrend
```

```
taper type cos width .3
cuterr fillz
cutim 0 10800
transfer from polezero subtype %GPPZ to none freq %f1 %f2 %f3
%f4
write %GPWRITE

*Broadband processing to transfer function
r %BROADBAND
cutim %TIME1BB %TIME2BB
rmean
rtrend
taper type cos width .3
cuterr fillz
cutim 0 10800
transfer from polezero subtype %BBPZ to none freq %f1 %f2 %f3
%f4
write %BBWRITE
```

#4: Filter and plot

```
*Time-Series comparison can be made by using a bandpass filter
*to compare signals between two frequencies
*After taking the 10 minute windows, a comparison can be made
*using the plot functions

*Variables that can be changed

*Files to be read in
setbb GEOPHONE Transfer.Geophone.SAC
setbb BROADBAND Transfer.Broadband.SAC

*Corners for bandpass corner frequencies and poles - Corners
*must be below the nyquist frequency
setbb c1 .03125
setbb c2 .125
setbb np 4

*Default removal
color off
xlim off
ylim off
qdp off
linlin
cuterr fillz


*To avoid artifacts from the bandpass filter, the 30 minute time
*window with zeros is used
*After bandpass is completed, files are cut down to smaller time
*windows for comparison

r %GEOPHONE
bp c %c1 %c2 n %np
cutim 600 1200
rmean
rtrend
write Geophone.Time_Series.SAC

r %BROADBAND
bp c %c1 %c2 n %np
cutim 600 1200
rmean
rtrend
*For IDOR, a amplitude discrepancy between the broadband and
*geophone requires an arbitrary constant adjustment
```

```
mul -52
write Broadband.Time_Series.SAC

*For the comparison, read in both files and plot parallel and
*superimposed
*For comparison, the braodband is colored blue and the geophone
*is colored red
color blue increment on list blue red
r Broadband.Time_Series.SAC Geophone.Time_Series.SAC
plot1
saveimg Parallel_Compare.ps
cutim 0 300
plot2
saveimg Superimpose_Compare.ps

*For correlation of the two signals, the data must be stretch
*so that the sampling rates match. There is risk of interpolated
*data producing errors in the waveforms.

r Broadband.Time_Series.SAC
stretch 5
write Stretch_Broadband.SAC

r Geophone.Time_Series.SAC
stretch 4
write Stretch_Geophone.SAC

r Stretch_Broadband.SAC Stretch_Geophone.SAC
correlate master 1 normalized
plot

write Autocorrelate.SAC CrossCorrelate.SAC
```

#5: Power Spectral Density

```
*For the spectral comparison of the sensors, the entire
*frequency range from the transfer function is used.
*Because of a lack of functionality for comparing images in the
*frequency domain using SAC, individual images can be created
*using the same plotting parameters, and plots can be overlayed
*using other imaging software.

*Variables needed for Power Spectral Density comparisons
*Files to read in:
setbb BROADBAND Transfer.Broadband.SAC
setbb GEOPHONE Transfer.Geophone.SAC

*Turn off defaults
xlim off
ylim off
color off
qdp off
linlin

r %BROADBAND
cutim 600 1200
rmean
rtrend
*Arbitrary constant correction due to instrument response
*correction differences
mul -52
taper type cos width .05
cutim 0 1800
fft
keepam
sqr
div 600
write Broadband_PSD.SAC
color blue
loglog
xlim .005 20
ylim 10e-23 10e-6
plot
saveimg Broadband_PSD.ps

r %GEOPHONE
cutim 600 1200
rmean
rtrend
taper type cos width .05
```

```
cutim 0 1800
fft
keepam
sqr
div 600
write Geophone_PSD.SAC
color red
loglog
xlim .005 20
ylim 10e-23 10e-6
plot
saveimg Geophone_PSD.ps
```